DELAMINATION DETECTION OF HMA AIRPORT PAVEMENTS WITH NDT DEVICES

By:
Manuel Celaya, Soheil Nazarian, Chetana Rao and Harold Von Quintus
FAA Airport Technology R&D Branch, AJP-6310
William J. Hughes Technical Center
Atlantic City International Airport, NJ 08405
USA
Phone: (609) 485-5198; Fax: (609) 485-4845
David.Brill@faa.gov
Nick.Subbotin@faa.gov

PRESENTED FOR THE
2010 FAA WORLDWIDE AIRPORT TECHNOLOGY TRANSFER CONFERENCE
Atlantic City, New Jersey, USA

April 2010

ABSTRACT

Sufficient bonding between the hot mix asphalt (HMA) layers is essential to ensure the desired structural capacity of a pavement. Delamination or debonding problems are particularly more severe on airfield pavements, due to higher traffic loads applied by aircrafts. Further progression of delamination may result in stripping of the lower layers due to the intrusion of moisture or may develop other dangerous distresses such as foreign object debris (FOD). Rapid nondestructive test (NDT) methods to determine the existence and extent of delamination in asphalt pavements are needed. In this paper, the existing NDT procedures and equipment that have the potential to address the problem were identified and their effectiveness and potential for success were evaluated. The identified NDT methods, which included the Ground Penetrating Radar, Thermography, sonic/seismic and impulse response, were evaluated on a controlled pavement section that was specifically constructed with various levels of debonding at different depths and with different asphalt mixes. The theoretical and practical strength and limitations of different methods are discussed in this paper.

INTRODUCTION

Sufficient bonding between pavement layers is essential for achieving the desired bearing capacity of a pavement. A poor bond and the subsequent delamination or debonding between the surfacing layers reduces the serviceability and performance of a pavement. The lack of interface bonding may lead to several premature distresses of which slippage, cracking, delamination and distortion are most prominent. Undetected delamination can ultimately result in the peeling away of thin lifts from the surface of the roadway (Road Management & Engineering Journal [1]).

Delamination in most cases occurs either at high temperatures or high loads (especially horizontal loads) or a combination of the two when there is a poor bond between the surface and binder courses, for example due to poor quality tack coat material or application. Special attention has to be given to areas where horizontal loads are the largest. Delamination or debonding problems are particularly more severe on airfield pavements, due to higher traffic loads applied by aircrafts. This situation is more critical on runways at the high-speed taxiway exits, where airplanes brake and turn (Bognacki et al. [2]), or at areas under large horizontal load of aircraft at takeoff, creating slippage due to inadequate bonding between the top layer and the layer below. Jet blasts can particularly complicate the problem by converting fragments of the delaminated layer into foreign object debris (FOD). Moreover, the delaminated layers and their associated cracks may require frequent maintenance, and may lead to premature need for major rehabilitation. For those reasons, rapid detection of delamination with NDT devices is desirable.

The objective of this paper is to evaluate the feasibility of estimating the presence and extent of HMA delamination with NDT methods. Selected NDT equipment and procedures that deemed capable of locating areas of delamination were tested and conclusions on their applicability were drawn. Four NDT methods were evaluated on a pavement section specifically constructed for this study. Several debonding agents were placed between different asphalt lifts at predetermined locations to simulate different degrees of debonding within the pavement.

In this paper, a brief literature review on the selected NDT methods for detection of delamination in HMA pavements is introduced. The pavement section constructed for this study

is described. Results obtained with selected NDT methods and the summary and conclusions of this study are presented.

NDT METHODS FOR DETECTING DELAMINATION OF HMA

A number of NDT technologies have been developed that can be potentially employed for detection of delamination within HMA layers. Most of these technologies have been used extensively for detecting the delamination in portland cement concrete (PCC) slabs. However, several complicating factors have to be addressed in applying these methods to HMA. These complications included the following items:

- PCC slabs are typically placed in thicker lifts than HMA layers,
- the cement paste generates an almost homogenous layer as opposed to the HMA that is essentially a particulate matter,
- the tack coat at the interface of successive HMA layer may act as a weak bonding agent, complicating the detection of debonding, and
- changes in temperature play a key role in the measured mechanical properties of HMA layers as well as the adhesion characteristics of tack coat that may affect the results.

The following four NDT methods that were considered most promising were preliminary evaluated in this study: 1) Ground Penetrating Radar (GPR), 2) Impulse Response (IR), 3) Ultrasonic Surface Waves (USW) and 4) Thermography. Even though not reported here for the sake of brevity, a Falling Weight Deflectometer (FWD) was also utilized. The results from FWD test were encouraging as discussed in Celaya et al. [3]. A brief description of each method is provided next.

Ground Penetrating Radar (GPR)

GPR is a geophysical nondestructive technique that uses electromagnetic pulses to test, characterize, or detect subsurface materials based on changes in electromagnetic properties of the subsurface layers. GPR has been extensively used for measuring pavement layer thicknesses (ASTM D4748), locating changes and anomalies in pavement structures, detecting voids under concrete slabs, locating reinforcement and dowels in jointed concrete pavements, and moisture damage (stripping) in asphalt pavements. The main advantage of the GPR is the speed of the operation and almost full-coverage of the pavement section. However, the application of GPR in detecting delamination has been found to be questionable. Even at frequencies of 1 to 2 GHz, the GPR wavelengths in asphalt are too long to resolve the thin delamination (Maser [4]). Numerical modeling of the GPR signals for detecting delaminated asphalt carried out by Smith and Scullion [5] indicated that the detection of an air-filled delamination of 0.2 in. thick or water-filled delamination of 0.1 in. and thicker at a minimum depth of 2 in. may be detectable using a 2.5 GHz GPR antenna at a maximum speed for data acquisition of 10 mph.

The test setup used in this study is shown in Figure 1. The equipment used consisted of a GSSI SIR-20 (SIRveyor) two-channel data acquisition unit controlled by a laptop computer, a 1.5 GHz ground-coupled antenna (GSSI Model 5100), and a survey wheel attached to the antenna. The maximum depth of penetration of this antenna is about 1.5 ft depending on the dielectric properties of the pavement.

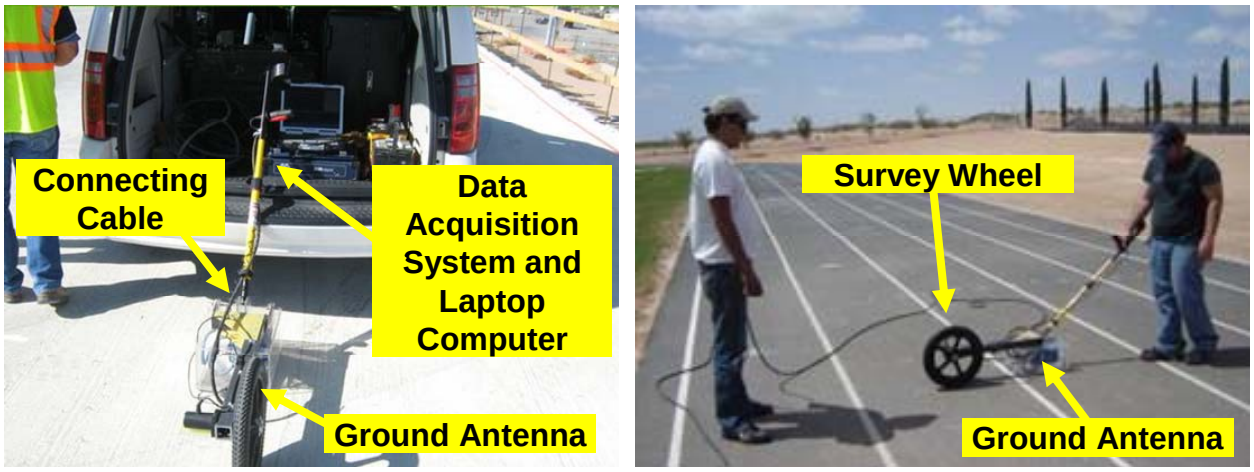

Figure 1. GSSI Model 5100 GPR System Used in This Study

Impulse Response (IR) Method

In the IR method, the deformation of the pavement is measured due to a known load. The basic operating principle of the method is to apply an impulsive loading to the pavement surface with an instrumented hammer and to measure the vertical displacement using a geophone. The impulse duration of less than 1 msec would result in predominant vibration of the top layer. If structural distresses are present in the form of loss of adhesion between pavement layers, this is reflected in the dynamic response of the pavement structure. By performing a simple modal analysis (Nazarian et al. [6]), the bonding condition of two adjacent layers can be determined. The same principle has been employed in several research studies aiming at characterizing the bond conditions below thin HMA surfacing (Lepert et al. [7]). Kruntcheva et al. [8] successfully implemented this method for detection of debonding in controlled test sections. The equipment used in this study is shown in Figure 2. A 10-lb (45 N) hammer instrumented with a load cell and a 4.5-Hz geophone were used. Both the hammer and the receiver were connected to a portable field computer for data acquisition and storage.

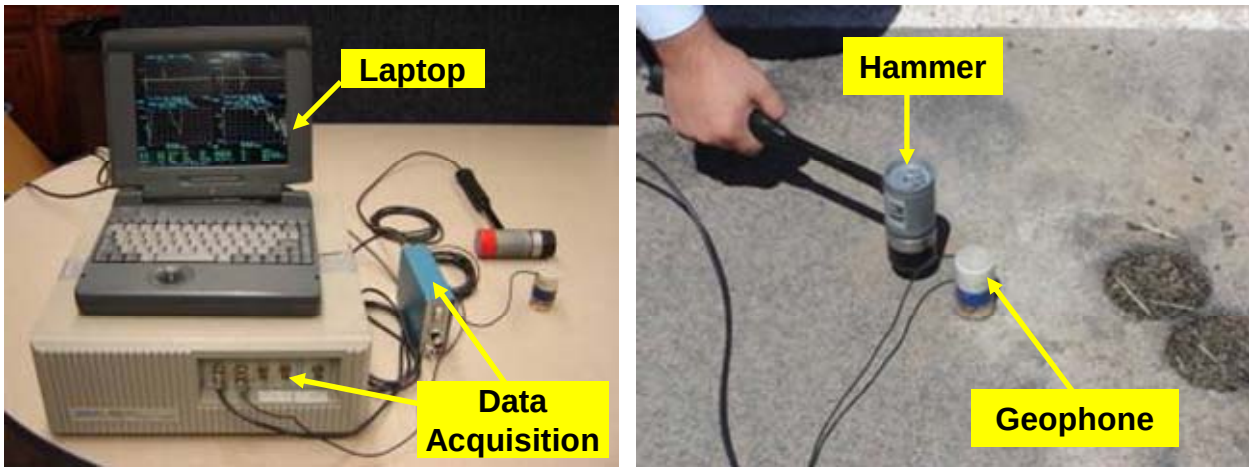

Figure 2. Impulse Response Test Setup

Ultrasonic Surface Waves (USW)

The USW is a seismic-based method, in which the variation in the velocity with wavelength is measured to generate a so-called dispersion curve. For two layers with similar modulus bonded together, the variation in modulus with wavelength is more or less constant. However, when the two layers are debonded, the modulus will decrease significantly with wavelength below the interface of the two layers. This method has been successfully used in forensic studies to detect HMA stripping (Hammons et al. [9]). The Portable Seismic Property Analyzer (PSPA) was used in this study. The PSPA (see Figure 3), which determines the variation in modulus with depth of the exposed layer in the field, consists of two ultrasonic sensors or transducers and a source packaged into a hand-portable system using the USW method (Nazarian et al. [10]). The PSPA is operable from a laptop computer. The computer is tethered to the hand-carried transducer unit through a cable that carries power to the hammer and transducers and returns the measured signals to the data acquisition board in the computer. The outputs of the two transducers are subjected to signal processing and spectral analyses. In the USW method, the surface or Rayleigh wave velocity, V_R, is measured without an inversion algorithm. After V_R is measured, the modulus of the top layer, E_{field}, can be determined from (Nazarian et al. [10]).

$$E_{field} = 2\rho\left[V_R\left(1.13 - 0.16\nu\right)\right]^2\left(1+\nu\right) \tag{1}$$

where ρ is mass density, and ν is Poisson's ratio.

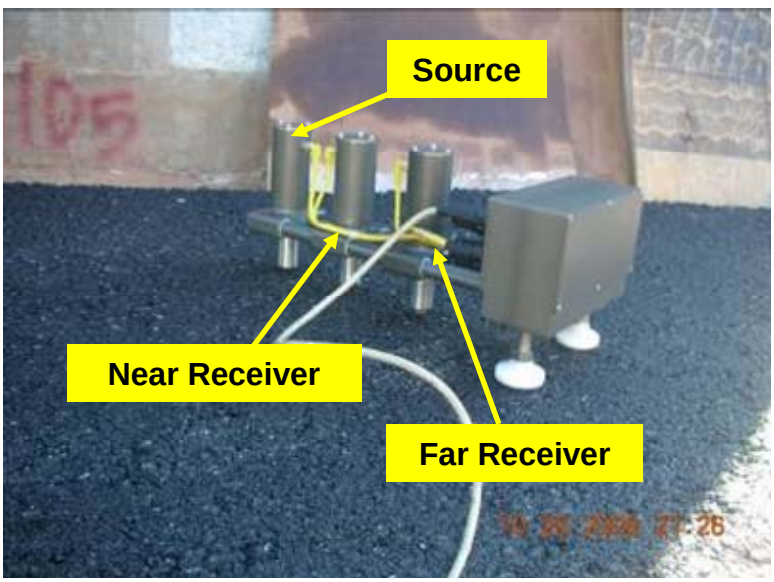

Figure 3. PSPA Detail

Thermography Method

Infrared Thermography measures temperature distributions across the surface of the pavement to detect the presence of shallow subsurface flaws in HMA. The surface of the pavement over a delaminated area exhibits a temperature gradient with respect to its surrounding fully-bonded area (Maser [11]). Stroup-Gardiner and Brown [12] showed that temperature differentials measured by thermography were also impacted by the changes in the properties of

the finished mat (such as air void content and gradation) that may negatively impact the reliability of this technology for the detection of delamination. Thermography has been used for detection of shallow delamination in HMA airfield pavements by Tsubokawa et al. [13] and Moropoulou et al. [14]. Both studies concluded the effectiveness of thermography for large areal inspection but also reported a number of limitations in term of its high sensitivity to ambient environmental and surface conditions such as solar radiations, air temperature, wind speeds, surface texture, the external debris, shadow zones, etc. An InfraCAM™ SD from FLIR systems was used in this study as shown in Figure 4. The camera collects thermal images of a surface area of approximately 2 ft by 2 ft (0.6 m by 0.6 mm) when the camera is used at a height of approximately 4 ft (1.2 m) from the surface. The operator aims a laser pointer to the surface of the pavement and collects and stores an image of 240x240 pixels.

Figure 4. Infrared Camera Used on This Study

CASE STUDY

Ten different sections were constructed specifically for this study as depicted in Figure 5. Each section was 9 ft long (2.7 m) by 10 ft (3 m) wide. Three transition zones were incorporated to minimize the variability of the laid down mix during construction. The pavement cross-section for all sections consisted of a prepared sandy-silt subgrade and about 8 in. (200 mm) of HMA placed in three lifts. The bottom lift consisted of about 3 in. (75 mm) of a coarse (P-403) mix and the middle lift 2.5 in. (63 mm) of a fine (P-401) mix. The top lift of Sections 1 through 5 consisted of a coarse mix (P-403 mix) and Sections 6 through 10 a fine mix (P-401 mix).

A typical plan view of each section and test locations are depicted in Figure 6. A 4 ft (1.2 m) by 9 ft (3 m) area for each section was intentionally debonded. In addition, smaller debonded areas were constructed to test the detectability threshold of the methods. For the study reported here, the focus was more on the 4 ft by 9 ft debonded areas.

To establish the suitability of different materials to be used as debonding agents, a series of direct shear tests were conducted. Clay slurry, talcum powder, grease and thin paper soaked in motor oil were considered. A tack coat in compliance with Item P-603 at a rate of 0.14 g/yd^2 (0.7

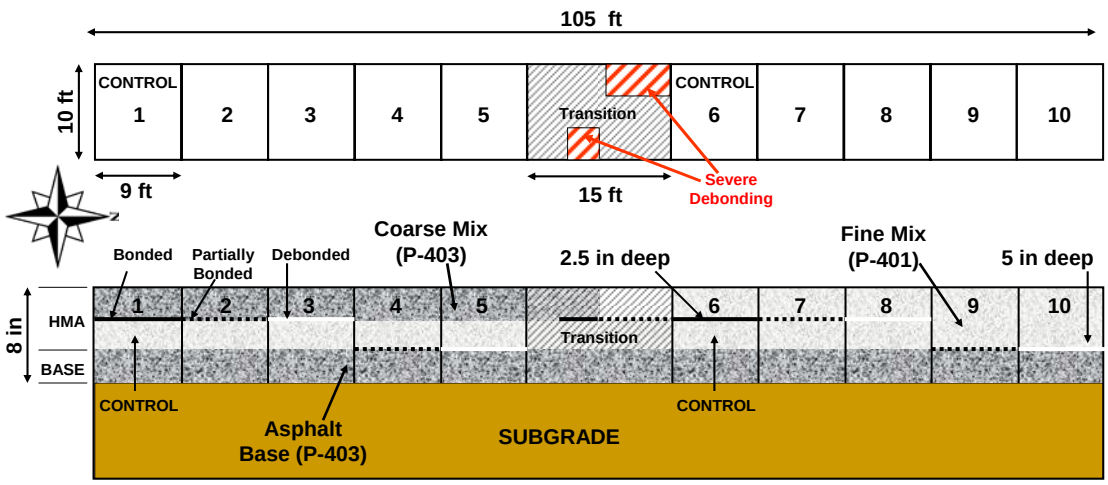

Figure 5. Schematic of Small Scale Section Constructed for this Study.

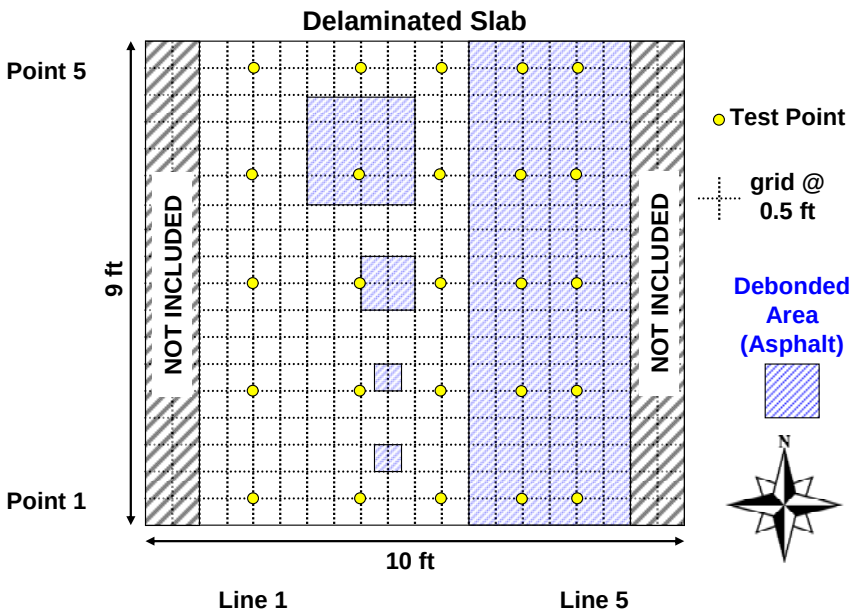

Figure 6. Location of Test Points for a Given Section.

lit/m^2) was used as the control bonding agent. The shear strengths measured for each bonding agent are presented in Table 1. Two sets of specimens were prepared. One set consisted of the P-403 mix as the bottom lift and the P-401 mix as the top lift. The other set comprised of two lifts of the P-401 mix. For both sets of specimens, the highest bond strengths were associated with the tack coat (about 33 psi, 220 kPa), and the lowest with a thin paper soaked in motor oil (about 5 psi, 35 kPa). The coefficients of variation (COVs) of the shear strengths are rather high which can be explained by the shear resistance from aggregate interaction. Based on the shear strength results, sections constructed with the tack coat were considered as fully-bonded. The sections with the clay slurry, talcum powder and grease were considered as partially-debonded, and those with oily paper as fully-debonded. A severely debonded area was reproduced in the transition area by placing a 4 by 4 ft (1.2 m by 1.2 m) piece of thick corrugated cardboard and a thick layer of clay slurry of 4 by 6 ft (1.2 m by 1.8 m) as shown in Figure 5. The characteristics of the

sections are summarized in Table 2. Shallow and deep correspond to the debonding between the top two lifts (at a depth of 2.5 in.) and bottom two lifts (a depth of 5 in.), respectively.

Table 1. Shear Strengths (in psi) for Laboratory Prepared Specimens.

Sample Condition	P-401/P-401 Mixes					P-403/P-401 Mixes			
	Tack Coat	Talcum Powder	Clay Slurry	Grease	Paper Soaked in Motor Oil	Tack Coat	Talcum Powder	Clay Slurry	Paper Soaked in Motor Oil
Average	35	20	22	19	5	32	17	27	5
COV	36%	51%	75%	19%	34%	24%	5%	19%	47%

Table 2. Characteristics of Sections Used in This Study.

Section**	Surface Mix	Designation	Debonding Agent				
			Tack Coat	Grease	Clay Slurry	Talcum Powder	Paper with Oil
1, 6	Coarse Mix	**Control**	√				
2, 7		**Shallow Partially-Debonded**		√	√		
3, 8		**Shallow Fully-Debonded**				√*	√
4, 9		**Deep Partially-Debonded**		√	√		
5, 10		**Deep Fully-Debonded**				√*	√

** Partially-Debonded*
*** Sections 1 through 5 with Coarse Surface Mix and Sections 6 through 10 with Fine Surface Mix*

PRESENTATION OF RESULTS

Ground Penetrating Radar

The linescans with the GPR system along Lines 1 (intact line) and 5 (containing debonded areas) along with the locations of the prepared debonding are shown in Figure 7. The interfaces of different HMA lifts are also shown. The reflections from the debonded areas should be easily observable because of the higher reflection amplitudes. The GPR detected the severely debonded area within the transition zone and some debonded areas primarily constructed on talcum powder or clay perhaps because of the significant contrasts in their dielectric constants and HMA. This indicates that the GPR may be most suitable when the debonding is in severe stages or when moisture is present along the interface of the debonded layers.

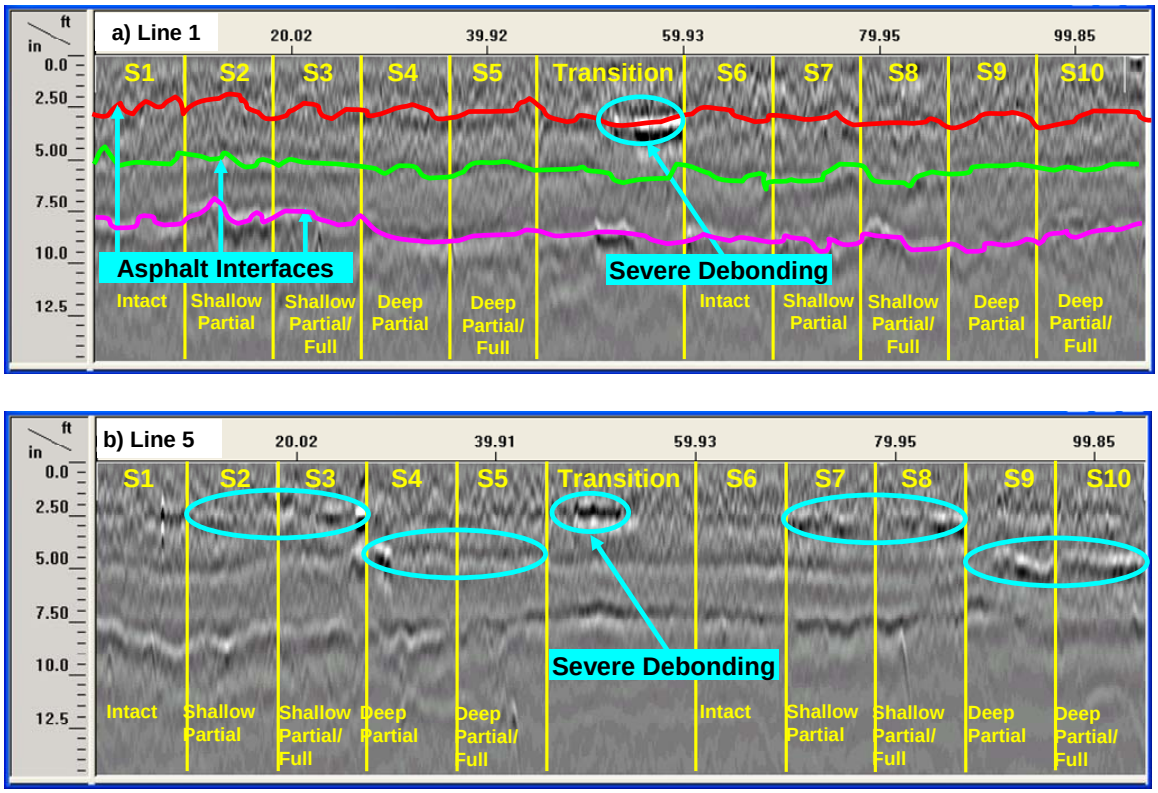

Figure 7. Linescans with Ground-coupled GPR along Line 1 (Intact) and Line 5 (Debonded).

Impulse Response

An example of two test results on a sound and severely debonded area are shown in Figure 8. The voltage amplitude of the geophone for the severe debonded area was around three to four times as large as compared to the intact location and also much wider, while the amplitude of the load remained similar (see Figures 8a and 8c). The ratio between the load cell and geophone amplitudes can be used initially because of its simplicity where smaller ratio corresponds to greater flexibility of the section and therefore debonded locations. A more appropriate but slightly more complicated analysis consisted on determining the frequency responses using a Fast-Fourier Transform (FFT) algorithm as presented in Figures 8b and 8d. For the intact location the amplitude presented a dominant frequency of 300 Hz with amplitude of 4.5 and for the severe debonded the frequency was erratic and the maximum amplitude was close to 30. The ratio of the maximum values of the FFT amplitudes (stiffness) was used to compare the results.

In this study, it was found that temperature at the time of testing greatly affected the outcome of this method in terms of FFT amplitudes. Therefore, several points were tested repeatedly at different times corresponding to different temperatures. The temperature adjustment relationship for Sections 1 and 6 are presented in Figure 9. The general equation to adjust stiffness is:

$$FFT_{77^\circ F} = \frac{FFT_{T^\circ F}}{-0.009 \cdot T + 1.69} \tag{1}$$

This relationship is very site specific and need to be developed for each site to be tested.

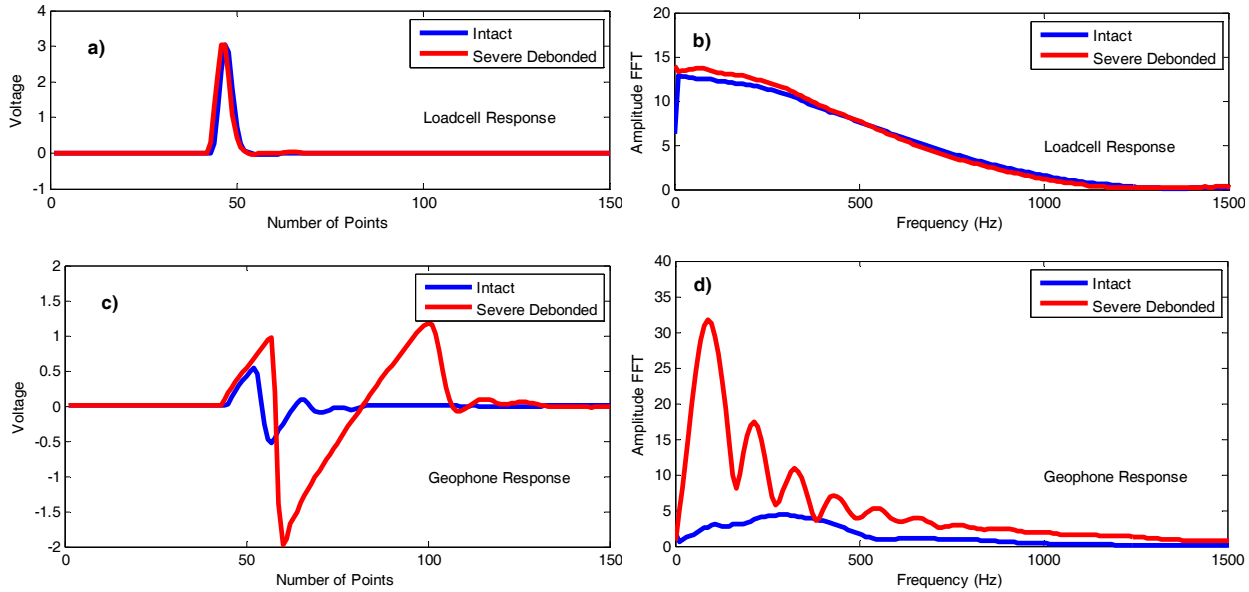

Figure 8. Time Records and FFT Results from IR Examples on Small Scale Study.

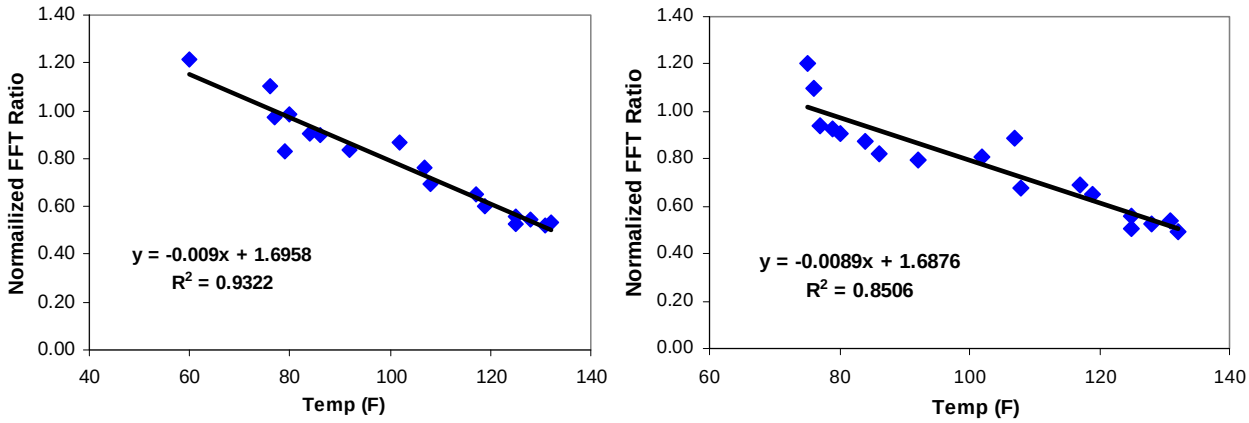

a) Surface Coarse Mixes b) Surface Fine Mixes

Figure 9. Influence of Temperature on IR FFT Amplitude Ratios (Stiffness).

The temperature adjusted stiffnesses were compared using color-coding in Figure 10. The average stiffness ($E_{control}$) and standard deviation ($\sigma_{control}$) of each control section (1 and 6) were used as reference. Stiffnesses above the average minus one standard deviation are colored as green, between average minus one and average minus two standard deviations are highlighted in yellow, and less than average minus two standard deviations are colored as red. In this case most of the fully debonded points along lines 4 and 5 were identified for both mixes. Some partially debonded areas showed indication of marginally less stiff (marked as yellow), but some were found to be intact (green) or substantially less stiff (red). Most of the intact locations (line 1 and sections 1 and 6) were identified as intact. Based on these preliminary results, the IR method seems promising for the detection of the fully-debonded areas both shallow and deep and some of the partially-debonded areas.

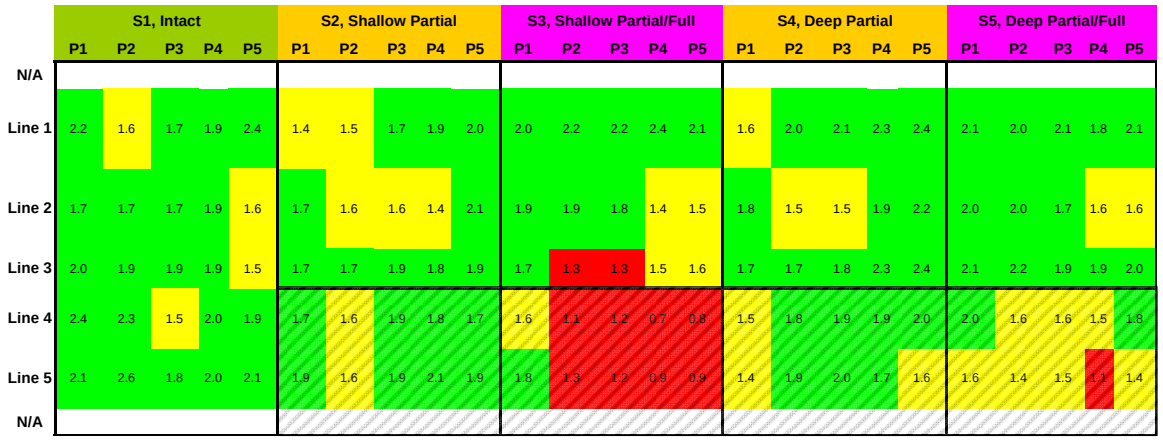

a) Sections 1 to 5

$E > E_{control} - \sigma_{control}$ | $E_{control} - \sigma_{control} > E > E_{control} - 2*\sigma_{control}$ | $E < E_{control} - 2*\sigma_{control}$

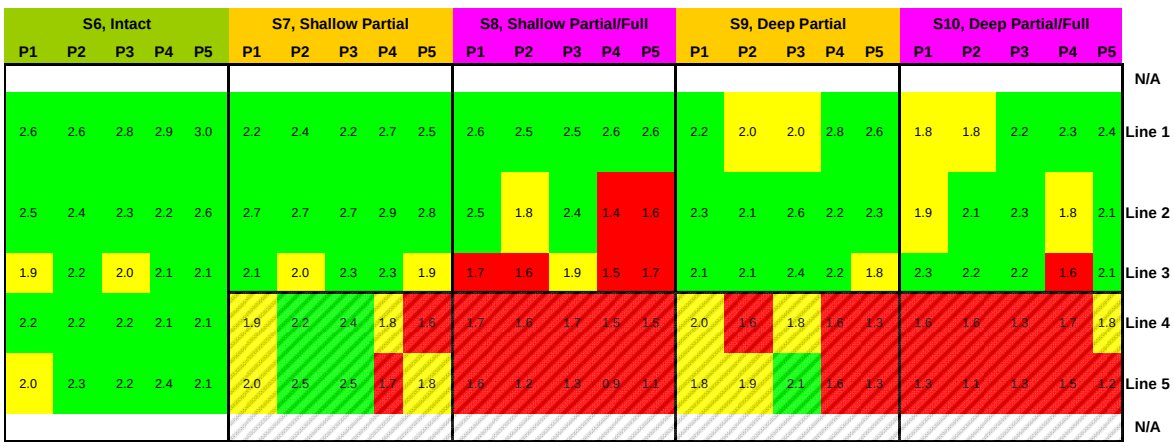

b) Sections 6 to 10

Figure 10. Representation of the Impulse Response Results.

Ultrasonic Surface Waves (USW) Method

The PSPA USW analysis pages as seen by the operator in the field are shown in Figure 11 for the intact and severely debonded locations. The top graphs demonstrate the variation in modulus with wavelength (called dispersion curves). The dispersion curve for the intact area is fairly uniform; whereas for the damaged point a sharp decrease in modulus below a wavelength of 2.5 in. (63 mm, the location of the damage) is evident. The vertical red lines in the graphs demonstrate the average moduli of the HMA layer from close to surface (1 in., 25 mm) to 8 in. (200 mm, nominal thickness of the layer). As reflected in the left hand side of the two graphs, the average moduli are about 1500 ksi (10 GPa) for the intact and 1130 ksi (7.8 GPa) for the severely-debonded areas.

The variation in the average moduli along the ten sections is color-coded in Figure 12 using the criteria used for the IR tests. Since HMA modulus is temperature dependent, the values presented were converted to a reference temperature of 77ºF using (Li and Nazarian, [15]):

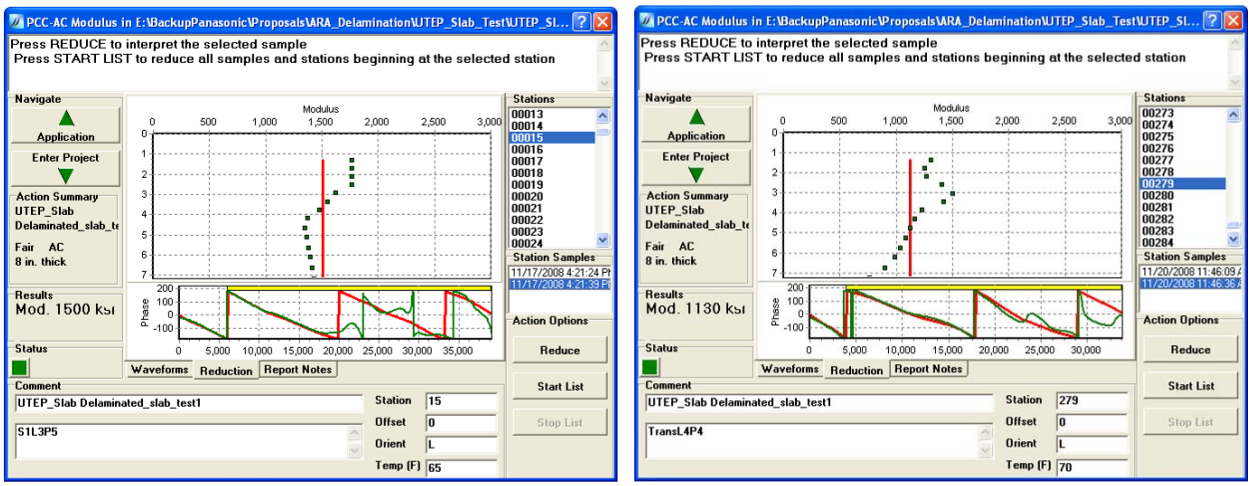

a) Intact b) Severe Debonding

Figure 11. Dispersion Curve Results with PSPA.

	S1, Intact					S2, Shallow Partial					S3, Shallow Partial/Full					S4, Deep Partial					S5, Deep Partial/Full				
	P1	P2	P3	P4	P5	P1	P2	P3	P4	P5	P1	P2	P3	P4	P5	P1	P2	P3	P4	P5	P1	P2	P3	P4	P5
N/A																									
Line 1	1768	1777	1812	1736	1991	2231	2236	1951	2214	1929	1983	1891	1956	1933	1633	1808	1955	1668	1724	1645	1666	1783	1914	1845	1733
Line 2	1921	1690	1714	1636	1829	1685	1957	1755	1778	1626	1874	1527	1611	1643	1347	1715	1729	1612	1502	1712	1827	1374	1879	1767	1851
Line 3	1674	1835	1854	1589	1825	1977	1807	1899	1974	1563	1908	2325	1617	1714	1747	1666	1815	1676	2025	1984	1651	1614	1684	1914	1652
Line 4	1602	1626	1963	1891	1751	1804	1643	1740	1768	1320	1289	987	1326	1266	1387	1453	1617	1696	1653	1837	1442	1573	1690	1599	1506
Line 5	1745	1699	1683	1876	1922	1902	1667	1626	1774	1149	1043	1151	1313	1054	1091	1044	1548	1726	1511	1437	1527	1264	1481	1421	1627
N/A																									

a) Sections 1 to 5

	S6, Intact					S7, Shallow Partial					S8, Shallow Partial/Full					S9, Deep Partial					S10, Deep Partial/Full					
	P1	P2	P3	P4	P5	P1	P2	P3	P4	P5	P1	P2	P3	P4	P5	P1	P2	P3	P4	P5	P1	P2	P3	P4	P5	
N/A																										N/A
Line 1	1443	2083	1809	1827	1717	1762	1824	1628	1727	1644	1598	1873	1524	1448	1869	1828	1882	1845	1655	1802	1873	1990	1760	1802	###	Line 1
Line 2	1953	2212	2095	2171	1962	1813	1819	1960	2023	1300	1719	1744	1856	1513	1469	1795	1741	1720	1753	1569	1899	1902	2356	1993	###	Line 2
Line 3	2134	1967	1828	1968	1569	1961	1750	1880	1854	1649	2051	2048	2335	1919	2141	1836	1825	1922	2050	1646	2117	2058	2234	2213	###	Line 3
Line 4	2116	2307	2175	2025	1924	1771	1766	1592	1847	1531	1578	1674	1667	1542	1629	1387	2140	2093	1986	1598	1888	2006	2073	2018	###	Line 4
Line 5	1990	2156	2078	2031	2180	1841	1680	1777	1611	1538	1612	1469	1409	1463	1375	1446	2034	1661	1820	1729	1557	1615	1572	1677	###	Line 5
N/A																										N/A

b) Sections 6 to 10

Figure 12. Statistical Analysis of PSPA Modulus on Small Scale Study.

$$Modulus_{77F} = \frac{Modulus_T}{(-0.00307 * T + 1.2627)} \quad (2)$$

In Figure 12a (representing coarse surface mix) an area from the right hand side of Section 2 until the end of Section 5 generally exhibits lower moduli as anticipated. However, parts of Sections 2 and 4, both located on partially debonded sections, exhibit normal moduli. Similar trends are observed for the fine surface HMA sections (Figure 12b). However, the deep debonding is not as well defined as for the similar sections with coarse surface HMA.

Detailed dispersion curves for Line 1 (intact) and Line 5 (primarily debonded) along the ten sections are presented in Figure 13 with prepared debonded areas marked when applicable. Reductions in modulus can be observed in most sections below depths of prepared debonding except for section 9 along Line 5 (deep partially-debonded section). Along Line 1, some reduction in modulus with depth is also observed, but to a much lesser extent than on the debonded areas, which can be attributed to the quality of the lower HMA layers. This demonstrates that the USW method might be able to identify delaminated areas reasonably well, especially the shallow ones.

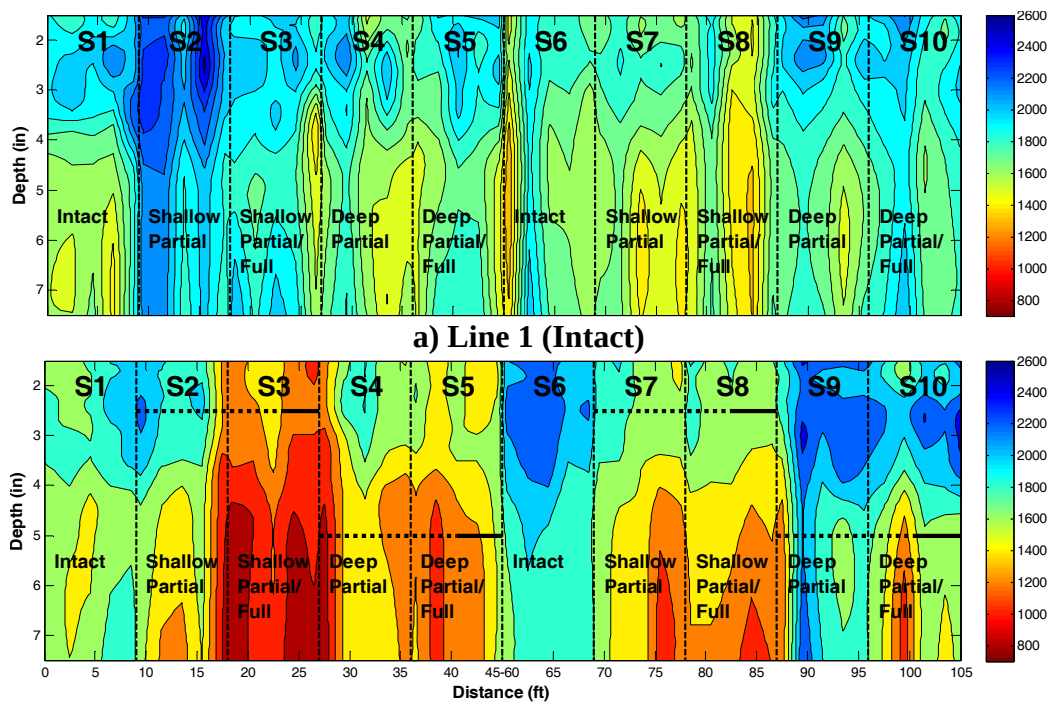

a) Line 1 (Intact)

b) Line 5 (Primarily Debonded)

Figure 13. Dispersion Curve Results for Lines 1 and 5.

Thermography

A combined image around the severely deboned area is shown in Figure 14. A passive source (sunlight) was used to create the temperature differentials on the surface. The hotter areas (depicted in white) correspond to the area on top of the severe debonding. The same procedure

was applied to collect the data on the ten sections. A total of 25 pictures were obtained on each section at the predetermined locations as shown in Figure 15. Only the severely debonded area within the transition zone was clearly detected by the infrared camera. The results of this method were not very encouraging. A more sensitive camera (with precision of better than 0.1 degree) may provide more reasonable results.

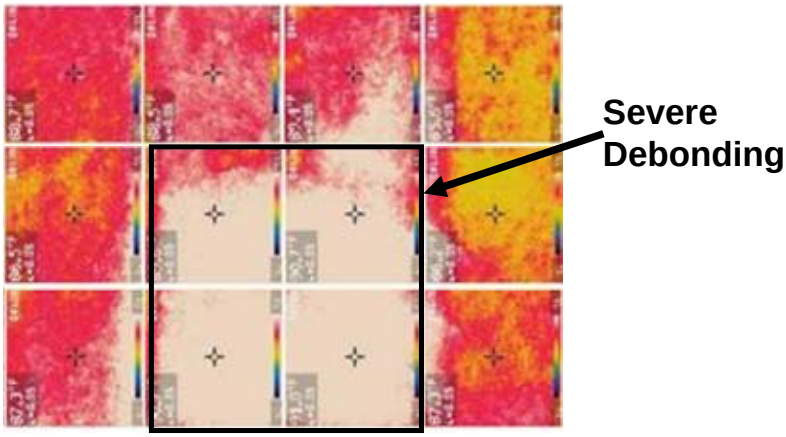

Figure 14. Infrared Camera Results on Severe Debonded Area.

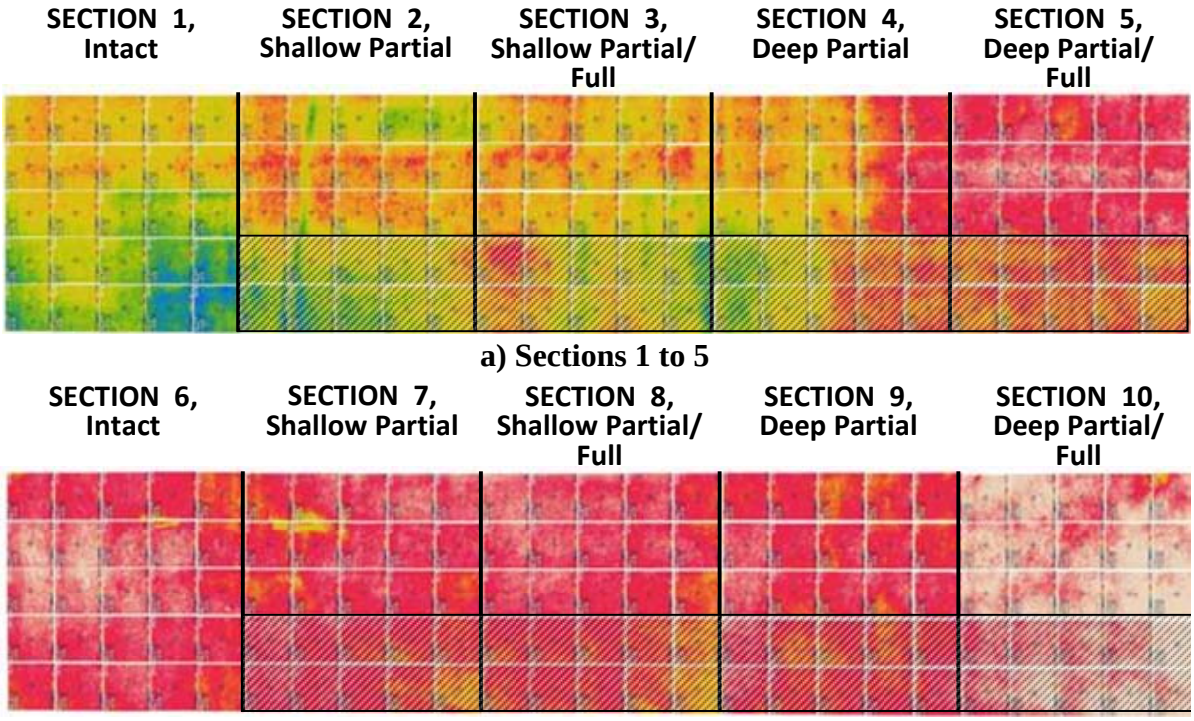

a) Sections 1 to 5

b) Sections 6 to 10

Figure 15. Infrared Camera Results on Small Scale Study.

CONCLUSIONS

Several NDT procedures and equipment that have the potential to detect the debonding of the HMA were evaluated. The NDT methods considered included the Ground Penetrating Radar,

impulse response, sonic/seismic, Thermography and the Falling Weight Deflectometer (FWD). A pavement section specifically constructed with various levels of debonding at different depths and with different asphalt mixes were used for this purpose. These five methods detected a severely debonded section well. Based on the outcome of the study, the following statements can be made:

- GPR could detect 33% of the debonded areas, primarily when talcum powder or clay was used as the debonding agent. GPR could be used as a qualitatively method to identify severely debonded areas, especially in the presence of moisture.

- The impulse-response method could detect about 59% of the debonded areas with the majority of defects detected were the fully-debonded areas (both shallow and deep). This method was the most successful in terms of detecting the fully-debonded defects.

- The USW method as implemented in the PSPA could detect 53% of the debonded areas. PSPA could detect the shallow debonding (both partial and full) the best.

- The thermography was not as successful in these experiments as reported in the literature. This method could only detect the severely debonded area in the transition.

- The FWD, even though not discussed here, could detect about 46% of the debonded areas based on the backcalculation of the modulus of the HMA layer.

- The IR, FWD and USW methods require temperature adjustments for their success. Approximate temperature adjustment relationships exist for the USW and FWD methods. However, for the IR a site specific temperature adjustment protocol may be needed.

A more comprehensive study with more data points and considering the environmental parameters (such as temperature) and the detectability threshold of the methods are underway that will be discussed in the future papers.

ACKNOWLEDGEMENTS

The authors wish to gratefully acknowledge the support of the Airfield Asphalt Pavement Technology Program (AAPTP).

REFERENCES

1. www.usroads.com/journals/rmj/9704/rm970403.htm. Road Management & Engineering Journal. Article Outlines Six Steps to Patching Potholes, April 1, 1997. *Website accessed February 2008.*
2. Bognacki, C. J., Frisvold, A. and Bennert, T. (2007), "Investigation of asphalt pavement slippage failures on Runway 4R-22L, Newark International Airport." FAA Worldwide Airport Technology Transfer Conference. Atlantic City, New Jersey, USA.
3. Celaya, M., Mejia, D., Ertem, S., Nazarian, S., Rao, C., Von Quintus, H. and Shokouhi, P. "Evaluation of NDT Technologies to Assess Presence and Extent of Delamination of HMA Airfield Pavements: Verification Study." AAPTP Report for Project 06-04, October 2009.

4. Maser K. R. (1996), “Condition assessment of transportation infrastructure using ground-penetrating radar”, ASCE Journal of Infrastructure Systems, pp. 94-101
5. Smith, S., S., Scullion, T. Development of Ground-Penetrating Radar Equipment for Detecting Pavement Condition for Preventive Maintenance. SHRP-H-672. Strategic Highway Research Program. National Research Council Washington, DC 1993.
6. Nazarian S., Reddy S. and Baker M. (1994), "Determination of voids under rigid pavements using impulse response method," STP 1198, ASTM, pp. 473-487, Philadelphia, PA.
7. Lepert, P., Poilane, J. P., and Villard-Bats, M. (1992). “Evaluation of various field measurement techniques for the assessment of pavement interface condition.” Proceedings, 7th International Conference on Asphalt Pavements, Vol. 3, 224–237.
8. Kruntcheva, M., R., Collop, A., C. and Thom, N., H. (2004) “Feasibility of assessing bond condition of asphalt concrete layers with dynamic nondestructive testing.” Journal of Transportation Engineering, Vol. 130, No. 4.
9. Hammons, M., I., Von Quintus, H., Maser, K., and Nazarian, S. (2005) “Detection of stripping in hot mix asphalt.” Applied Research Associates Project Number 16355, prepared for: Office of Materials and Research, Georgia Department of Transportation.
10. Nazarian, S., Yuan, D., Smith, K., Ansari, F., Gonzalez, C., “Acceptance Criteria of Airfield Concrete Pavement Using Seismic and Maturity Concepts. “Innovative Pavement Research Foundation, Airport Concrete Pavement Technology Program. Report IPRF-01-G-002-02-2, May 2006.
11. Maser K.R. (2003). “Active Heating infrared thermography for detection of subsurface bridge deck deterioration,” Report NCHRP-IDEA Project 101, TRB, Washington, DC, 30 p.
12. Stroup-Gardiner M. and Brown E.R. (2000), “Segregation in hot-mix asphalt pavements”, NCHRP Report 441, TRB, National Research Council, Washington, D.C.
13. Tsubokawa, Y., Mizukami, J., Esaki, T., and Hayano, K. (2007) “Study on infrared thermographic inspection of de-bonded layer of airport flexible pavement.” FAA Worldwide Airport Technology Transfer Conference. Atlantic City, New Jersey.
14. Moropoulou, A., Avdelidis, N., P., Koui, M., and Kakaras, K. (2002) “Flaw detection and evaluation of airport pavements by means of infrared thermography.” http://www.flirthermography.com/media/Detection_Evaluation_Airport_Paving.pdf
15. Li, Y., and Nazarian, S. (1994), “Evaluation of Aging of Hot-Mix Asphalt Using Wave Propagation Techniques,” Engineering Properties of Asphalt Mixtures And the Relationship to Their Performance, ASTM STP 1265, Philadelphia, Pa., pp.166-179.